Algorithm for Global Leaf Area Index Retrieval Using Satellite Imagery

Feng Deng, Jing M. Chen, Stephen Plummer, Mingzhen Chen, and Jan Pisek

***Abstract*—Leaf area index (LAI) is one of the most important Earth surface parameters in modeling ecosystems and their interaction with climate. Based on a geometrical optical model (Four-Scale) and LAI algorithms previously derived for Canada-wide applications, this paper presents a new algorithm for the global retrieval of LAI where the bidirectional reflectance distribution function (BRDF) is considered explicitly in the algorithm and hence removing the need of doing BRDF corrections and normalizations to the input images. The core problem of integrating BRDF into the LAI algorithm is that nonlinear BRDF kernels that are used to relate spectral reflectances to LAI are also LAI dependent, and no analytical solution is found to derive directly LAI from reflectance data. This problem is solved through developing a simple iteration procedure. The relationships between LAI and reflectances of various spectral bands (red, near infrared, and short-wave infrared) are simulated with Four-Scale with a multiple scattering scheme. Based on the model simulations, the key coefficients in the BRDF kernels are fitted with Chebyshev polynomials of the second kind. Spectral indices, the Simple Ratio and the Reduced Simple Ratio, are used to effectively combine the spectral bands for LAI retrieval. Example regional and global LAI maps are produced. Accuracy assessment on a Canada-wide LAI map is made in comparison with a previously validated 1998 LAI map and ground measurements made in seven Landsat scenes.**

***Index Terms*—Bidirectional reflectance distribution function (BRDF), Chebyshev polynomials, geometrical optical (GO) model, leaf area index (LAI), look-up table (LUT).**

I. Introduction

Satellite earth observation is a powerful tool to measure and characterize the state of the biosphere at regional and global scales. However, for quantitative applications of Earth observation data, we need to relate satellite spectral measurements to surface biophysical parameters, such as the leaf area index (LAI), and the fraction of absorbed photosynthetically active radiation (f_{APAR}). LAI is one of the key vegetation structural variables for quantitative analysis of many physical and biological processes related to vegetation dynamics and its effects on global carbon cycle and climate [1].

Manuscript received December 2, 2004; revised December 18, 2005. This work was supported in part by the European Space Agency.

F. Deng and J. Pisek are with the Department of Geography and Program in Planning, University of Toronto, Toronto, ON M5S 3G3, Canada.

J. M. Chen is with the Department of Geography and Program in Planning, University of Toronto, Toronto, ON M5S 3G3, Canada and also with York University, Toronto, ON M3J 1P3, Canada (e-mail: chenj@geog.utoronto.ca).

S. Plummer is with the IGBP-ESA Networks Initiative, ESA-ESRIN, Via Galileo Galilei, Frascati 00044, Italy.

M. Chen is with the Department of Geography and Program in Planning, University of Toronto, Toronto, ON M5S 3G3, Canada and also with the Auburn University, Auburn, AL 36849 USA.

Digital Object Identifier 10.1109/TGRS.2006.872100

Following the Advanced Very High Resolution Radiometer (AVHRR) series onboard National Oceanic and Atmospheric Administration (NOAA) satellites, VEGETATION onboard SPOT 4, the second Along-Track Scanning Radiometer (ATSR-2) on ERS-2, the Advanced ATSR (AATSR) and Medium Resolution Imaging Spectrometer (MERIS) onboard ENVISAT, and MODerate Resolution Imaging Spectroradiometer (MODIS) onboard Terra and Aqua satellites have been able to monitor the photosynthetic activity of the biosphere at regional and global scales at daily time intervals. However, with the available spectral measurements from these satellite sensors, two kinds of methods are often applied to estimating LAI. The first kind is based on vegetation indices (VIs), i.e., various combinations of reflectances in different spectral bands. Besides the most often used VIs, namely, Normalized Difference Vegetation Index (NDVI) [2], and Simple Ratio (SR) [3], a large number of other indices (e.g., [4]–[6]) have been used to relate LAI to surface reflectances. Based on VIs, algorithms were developed to estimate LAI from the reflectance of near-infrared (NIR), visible, and other spectral bands and regional and global maps [7]–[12] of LAI, and related products have been produced with various degrees of accuracy, although the problem of saturations of reflectances in the various spectral bands at high LAI values [13], [14] is always a major cause for concern using these data.

The alternative approaches are based on the inversion of canopy radiation models [13]. Because these models simulate physical processes, their derived parameters have physical meanings; thus, theoretically, these kinds of methods are preferable for our accuracy requirements. However, these methods require significant computational resources, and although they have become an interesting subject of current studies (e.g., [14], [15]), they are often too slow for global applications. This problem results not only from the complexity of canopy–radiation interaction processes but also from inversion methods themselves, which often require a large number of iterations to converge toward appropriate solutions. Besides the traditional iterative optimization approach, alternative methods such as look-up tables (LUTs) have been proposed for large dataset processing [16], [17]. The accuracy, however, depends on the dimension of the LUTs because very large LUTs will also slow down the search process. Therefore, a preferred inversion method for large-area applications would be LUTs with small or moderate dimensions requiring only few iterations.

As one of the main products of the MODIS sensor, the MODIS LAI product (MOD15A2) has been routinely produced and increasingly used for various global and regional studies [18], [19]. In the meantime, there are still issues related to the existing various datasets and algorithms, such as different definitions of LAI, different measurement instruments and protocols, different consideration of nonrandom canopy architecture, different cover type separations, different seasonal trajectory smoothing methods, etc. [9], [20]. Unfortunately, such LAI products can vary significantly depending on the algorithms (often developed based on specific radiative transfer models) and the input datasets used; thus, it is desirable to have alternative products for global and regional applications. One example of a regional alternative to MODIS is the Canada-wide LAI estimate [9]. However, this product is based on an algorithm that requires atmospherically corrected and bidirectional reflectance distribution function (BRDF)-normalized reflectance images, i.e., the atmospherically corrected reflectance images are normalized to a common geometry: nadir view and 45° solar zenith angle (SZA) [21]. For global applications, this BRDF normalization is not the ideal way to consider the angular effects because the SZA varies significantly globally for any given date and large normalization errors can therefore occur when we force the reflectance to a common SZA. This is particularly of concern as kernel-based simple BRDF models are often used for such normalization. For this reason and for global application, we change the approach by incorporating directly the effects of the BRDF and hence remove the requirement of BRDF normalization to the input images. The new algorithm is developed based on the Four-Scale bidirectional reflectance model [22]. For every land cover type, a large number of Four-Scale simulations are made to determine all the parameters of the algorithm, including BRDF kernel coefficients. Besides the conventional red and NIR bands, the short-wave infrared (SWIR) band is also used in the algorithm to replicate better the behavior of the vegetation reflectance in satellite images. A small LUT and a method that requires only two iterations are then compiled to accelerate the LAI inversion and make the algorithm applicable for processing global datasets.

The objectives of this article are 1) to document the principles of this new algorithm and 2) to validate the algorithm by comparing with a previously validated Canada-wide LAI image and ground measurements of different biomes in Canada. We will also show example global LAI products generated using this algorithm from the 10-day synthesis VEGETATION reflectance images at 1-km resolution.

II. Theoretical Basis

A. LAI Definition and Selection of a Spectral Index

LAI is defined as one-half the total green leaf area (all sided) per unit ground surface area [23]. This definition is the same as the traditional definition [24] based on the largest projected area (i.e., one sided) for broad leaves, but it makes a large difference for conifer needles.

As in most studies (see [27]), the LAI in this algorithm is estimated from remote sensing data using relationships between LAI and VIs. In our algorithm, we generally use the SR, defined as

$$\mathrm{SR} = \frac{\rho_{\mathrm{NIR}}}{\rho_{\mathrm{RED}}} \tag{1}$$

where ρ_{NIR} and ρ_{RED} are the reflectances in NIR and red bands, respectively. The relationship is developed based on Four-Scale simulations and can be expressed as

$$L = f_{\mathrm{L\_SR}}(\mathrm{SR} \cdot f_{\mathrm{BRDF}}(\theta_v, \theta_s, \phi)) \tag{2}$$

where L is the LAI, SR is the simple ratio, θ_s is the SZA, θ_v is the view zenith angle (VZA), ϕ is the relative azimuth angle between the sun and the viewer (PHI), $f_{\mathrm{L\_SR}}()$ is a function describing the relationship between BRDF-modified SR and LAI, and $f_{\mathrm{BRDF}}()$ is the BRDF modification function for SR.

A new vegetation index, the Reduced Simple Ratio (RSR) [25], which is less sensitive to vegetation type and background, was also used for specific vegetation types. It is defined as follows:

$$\mathrm{RSR} = \frac{\rho_{\mathrm{NIR}}}{\rho_{\mathrm{RED}}}\left(1 - \frac{\rho_{\mathrm{SWIR}} - \rho_{\mathrm{SWIR\,min}}}{\rho_{\mathrm{SWIR\,max}} - \rho_{\mathrm{SWIR\,min}}}\right) \tag{3}$$

where ρ_{SWIR} is the reflectance in the SWIR band and $\rho_{\mathrm{SWIR\,max}}$ and $\rho_{\mathrm{SWIR\,min}}$ are respectively the maximum and minimum SWIR reflectances selected for specific land covers.

Similarly, we establish a relationship between RSR and LAI based on the Four-Scale model

$$L = f_{\mathrm{L\_RSR}}\Bigg(\mathrm{SR} \cdot f_{\mathrm{BRDF}}(\theta_v, \theta_s, \phi) \cdot \left(1 - \frac{\rho_{\mathrm{SWIR}} \cdot f_{\mathrm{SWIR\_BRDF}}(\theta_v, \theta_s, \phi) - \rho_{\mathrm{SWIR\,min}}}{\rho_{\mathrm{SWIR\,max}} - \rho_{\mathrm{SWIR\,min}}}\right)\Bigg) \tag{4}$$

where $f_{\mathrm{L\_RSR}}()$ is a function describing the relationship between BRDF-modified RSR and LAI and $f_{\mathrm{SWIR\_BRDF}}()$ is a BRDF modification function for SWIR reflectance.

B. Canopy Reflectance Model Used

A physically based geometrical optical (GO) model is used here to simulate the interaction between incoming solar radiation and the vegetated surface and thus to generate parameters required for the LAI algorithm. The advantages of GO models relative to more sophisticated radiative transfer models (see review by Qin and Liang [26]) include their computation efficiency, easiness in investigating BRDFs for a large set of input parameters, and satisfactory accuracies for general applications [27]. The Four-Scale model developed by Chen and Leblanc [28] describes canopy reflectance considering four scales of canopy architecture including the distribution of tree crowns, crown geometry, crown internal structure (branches, shoots), and leaf distriubtion. The model used here also includes a multiple scattering scheme developed by Chen and Leblanc, and thus, it is also accurate for spectral bands (such as NIR and SWIR) with large multiple scattering effects in the canopy. In Four-Scale, the following theoretical expression for the hotspot shape is unique in utilizing the canopy gap size distribution information:

$$F(\xi) = \frac{\int_{\lambda_{\min}}^{\infty} \left[1 - \frac{\xi}{\tan^{-1}\left(\frac{\lambda}{H_\theta}\right)}\right] N(\lambda) d\lambda}{\int_{\lambda_{\min}}^{\infty} N(\lambda) d\lambda} \tag{5}$$

where ξ is the angle between the sun and the viewer relative to the target, defined as

$$\cos\xi = \cos\theta_s \cos\theta_v + \sin\theta_s \sin\theta_v \cos\phi \tag{6}$$

where $F(\xi)$ is a hot spot function, being unity when $\xi = 0$ and zero when ξ exceeds the largest $\tan^{-1}(\lambda/H_\theta)$ possible, H_θ is the gap depth in the direction of θ_s, $\lambda_{\min}$ is the smallest gap to be included in the integration and depends on the value of ξ, and $N(\lambda)$ is the number density for canopy gaps of size λ. $N(\lambda)$ is defined by

$$N(\lambda) = \frac{L_p}{W_p} \exp\left[-L_p \left(\frac{1+\lambda}{W_p}\right)\right] \tag{7}$$

where L_p is the projected area index of the objects responsible for the canopy gaps and W_p is the characteristic dimension of the objects.

The input parameters of Four-Scale can be separated in three categories, as follows:

1) site parameters (model domain size, LAI, tree density, tree grouping index, and SZA);
2) tree architectural parameters (crown radius and height, apex angle, needle-to-shoot ratio, and typical leaf or shoot size);
3) spectral reflectivities of the foliage and the background in the various bands.

Four-Scale is used to simulate BRDF shapes and relationships between BRDF and LAI for each of the major cover types using a large combination of these parameters. For LAI algorithm development, these simulated results are fitted with a kernel-based BRDF model as outlined below.

III. LAI Algorithm and Implementation Procedures

A. Algorithm Development

The Four-scale model is, however, too complex to be inverted directly on remote sensing images. Simplifications into combinations of four [29], [30] and two [31] kernels have been developed for various applications. In our LAI algorithm development, the two-kernel version, a modified Roujean's model [31], [32], is used as a base to fit the behavior of Four-Scale, i.e.,

$$\rho(\theta_v, \theta_s, \phi) = \rho_0(0,0,\phi)\left(1 + a_1 f_1(\theta_v,\theta_s,\phi) + a_2 f_2(\theta_v,\theta_s,\phi)\right) \cdot \left(1 + c_1 \exp\left[-\left(\frac{\xi}{\pi}\right) c_2\right]\right). \tag{8}$$

The last term involving c_1 and c_2 is the modification made by Chen and Cihlar to consider pronounced hotspot effects, based on the hotspot function as used by Four-Scale (5), although it introduces two additional parameters and makes the equation nonlinear. Functions f_1 and f_2 in (8) are defined as

$$\begin{aligned} f_1(\theta_v,\theta_s,\phi) &= \frac{1}{2\pi}\left[(\pi-\phi)\cos\phi + \sin\phi\right]\tan\theta_s \tan\theta_v - \frac{1}{\pi} \\ &\quad \cdot \Big(\tan\theta_s + \tan\theta_v \\ &\qquad + \sqrt{\tan^2\theta_s + \tan^2\theta_v - 2\tan\theta_s\tan\theta_v\cos\phi}\Big) \end{aligned} \tag{9}$$

and

$$f_2(\theta_v,\theta_s,\phi) = \frac{4}{3\pi}\frac{1}{\cos\theta_s + \cos\theta_v} \cdot \left[\left(\frac{\pi}{2} - \xi\right)\cos\xi + \sin\xi\right] - \frac{1}{3}. \tag{10}$$

In processing reflectance images, for any selected pixel in the image, the reflectance ρ_i and the angle combination $(\theta_{vi}, \theta_{si}, \phi_i)$ can be obtained, and with given values of a_1, a_2, c_1, and c_2, $\rho_0(0,0,\phi)$ can be calculated from the aforementioned formulas. Conversely, from $\rho_0(0,0,\phi)$, the reflectance ρ at any angle combination $(\theta_v, \theta_s, \phi)$ can also be estimated from (8). All of the BRDF kernel coefficients a_1, a_2, c_1, and c_2 are based on Four-Scale model results for different land cover types.

Given these relations, it is possible to write the functions f_{BRDF} and $f_{\mathrm{SWIR\_BRDF}}$ [(11) and (12), respectively, shown at the bottom of the next page] that can be used to cast the SR and SWIR bands of a pixel at any angle combination $(\theta_{vi}, \theta_{si}, \phi_i)$ to a new angle combination $(\theta_{vn}, \theta_{sn}, \phi_n)$: where subscript i represents an image pixel, subscript n represents the new angle combination from which we intend to calculate the LAI value given the LAI–SR or RSR relationship at that angle combination, and subscripts RED, NIR, and SWIR represent corresponding spectral bands.

In principle, based on (11) and (12), the LAI value can be calculated straightforwardly from (2) or (4). However, a complication exists because the kernel coefficients (a_1 and a_2) depend on the LAI to be retrieved. Thus, the core problem of integrating BRDF into LAI algorithm is that the equations describing the BRDF–LAI interdependence are functional relationships. Mathematically, this can be expressed, for SR- and RSR-based methods, respectively, as:

$$L = f_{\mathrm{L\_SR}}\left(\mathrm{SR} \cdot f_{\mathrm{BRDF}}\left(\theta_v, \theta_s, \phi, a_1(L), a_2(L)\right)\right) \tag{13}$$

and (14) (see equation at bottom of the next page).

Although this problem can be solved numerically, such methods are, however, not practical for large-area applications, which require computation efficiency. To make LAI retrieval feasible globally, we have developed a computational methodology to solve this problem through a simple iteration procedure. An alternative to this approach, the Secant method [33], in finding the proper L value was about seven times longer in computation time than the method we propose.

In our method, a precursor LAI value for a pixel is first produced from a general cover type-dependent SR–LAI relationship (2) assuming $f_{\mathrm{BRDF}}(\theta_{vi}, \theta_{si}, \phi_i) = 1$, then BRDF kernels parameters are calculated with this precursor LAI value, BRDF modification functions for SR and SWIR are calculated using (11) and (12), and finally, LAI is recalculated from the BRDF kernels and SR or RSR from (2) and (4). In practice, functions $a_1(L)$ and $a_2(L)$ and parameters c_1 and c_2 are prerequisites to using (13) and (14) for converting reflectances and SR from one angle combination to another. In our case, the functions $a_1(L)$ and $a_2(L)$ are expressed as Chebyshev polynomials of the second kind.

B. Chebyshev Polynomials Used in the Algorithm

In the process of algorithm development, a mathematical form is needed to express the relationships used in the algorithm that are both accurate and easily implemented. Chebyshev polynomials of the second kind [34] are chosen for this purpose. First, several Chebyshev polynomials $U_i(x)$ of the second kind for $x \in [-1, 1]$ and $i = 1, 2, 3, \ldots$ are defined as

$$\begin{aligned} U_0 &= 1 \\ U_1 &= 2x \\ U_2 &= 4x^2 - 1 \\ U_3 &= 8x^2 - 4x \end{aligned} \tag{15}$$

These can be expressed in a general recursive form, i.e.,

$$U_{i+1} = 2x.U_i - U_{i-1}. \tag{16}$$

In our LAI algorithm, the functions $f_{\mathrm{L\_SR}}$, $f_{\mathrm{L\_RSR}}$, $a_1(L)$, and $a_2(L)$ are represented in the recursive form

$$f = \sum_{i=0}^{i=n} k_i U_i(x), \qquad \text{for n} < 10 \tag{17}$$

where k_i are constants to be found from model results through regression analysis, and we found that 11 terms is sufficient to mimic any curve shapes from our simulations ($n < 10$). For example, x can be LAI, and f can be $a_2(L)$.

C. Cover Type-Dependent Algorithms

As vegetation structure is distinctly different among land cover types, Four-Scale simulations are made separately for different cover types. The functions $f_{\mathrm{L\_SR}}$ and $f_{\mathrm{L\_RSR}}$ and coefficients $a_1(L)$ and $a_2(L)$ are derived based on the simulations for each distinct cover type. In the implementation of the algorithm, any land cover map can be used, but in our case, we adopted the IGBP land cover map [35] and GLC2000 [36] although combining some of the cover types with similar structural characteristics as in Table I. Snow/ice and water body classes are not considered in LAI retrieval.

TABLE I
IGBP LAND COVER CLASSES AND COMBINED CLASSES FOR LAI RETRIEVAL

IGBP Class	Class Name	Combined Class
1	Evergreen needleleaf forest	Coniferous
2	Evergreen broadleaf forest	Tropical broadleaf(tropical region) Broadleaf mixed
3	Deciduous needleleaf forest	Coniferous
4	Deciduous broadleaf forest	Deciduous
5	Mixed forest	Mixed Forest (Coniferous, Deciduous)
6	Closed shrublands	Shrub
7	Open shrublands	Shrub
8	Woody savannas	Shrub
9	Savannas	Crop, Grass, and Others
10	Grasslands	Crop, Grass, and Others
11	Permanent wetlands	Crop, Grass, and Others
12	Croplands	Crop, Grass, and Others
13	Urban and built-up	Crop, Grass, and Others
14	Cropland mosaics	Crop, Grass, and Others
15	Snow/Ice	
16	Barren or sparsely vegetated	Crop, Grass, and Others
17	Water bodies	

$$f_{\mathrm{BRDF}} = \frac{(1 + a_{1\mathrm{RED}} f_1(\theta_{vi}, \theta_{si}, \phi_i) + a_{2\mathrm{RED}} f_2(\theta_{vi}, \theta_{si}, \phi_i)) \cdot \left(1 + c_{1\mathrm{RED}} \exp\left[-\left(\frac{\xi_i}{\pi}\right) c_{2\mathrm{RED}}\right]\right)}{(1 + a_{1\mathrm{NIR}} f_1(\theta_{vi}, \theta_{si}, \phi_i) + a_{2\mathrm{NIR}} f_2(\theta_{vi}, \theta_{si}, \phi_i)) \cdot \left(1 + c_{1\mathrm{NIR}} \exp\left[-\left(\frac{\xi_i}{\pi}\right) c_{2\mathrm{NIR}}\right]\right)} \cdot \frac{(1 + a_{1\mathrm{NIR}} f_1(\theta_{vn}, \theta_{sn}, \phi_{sn}) + a_{2\mathrm{NIR}} f_2(\theta_{vn}, \theta_{sn}, \phi_{sn})) \cdot \left(1 + c_{1\mathrm{NIR}} \exp\left[-\left(\frac{\xi_i}{\pi}\right) c_{2\mathrm{NIR}}\right]\right)}{(1 + a_{1\mathrm{RED}} f_1(\theta_{vn}, \theta_{sn}, \phi_{sn}) + a_{2\mathrm{RED}} f_2(\theta_{vn}, \theta_{sn}, \phi_{sn})) \cdot \left(1 + c_{1\mathrm{RED}} \exp\left[-\left(\frac{\xi_n}{\pi}\right) c_{2\mathrm{RED}}\right]\right)} \tag{11}$$

$$f_{\mathrm{SWIR\_BRDF}} = \frac{(1 + a_{1\mathrm{SWIR}} f_1(\theta_{vn}, \theta_{sn}, \phi_{sn}) + a_{2\mathrm{SWIR}} f_2(\theta_{vn}, \theta_{sn}, \phi_{sn})) \cdot \left(1 + c_{1\mathrm{SWIR}} \exp\left[-\left(\frac{xi_n}{\pi}\right) c_{2\mathrm{SWIR}}\right]\right)}{(1 + a_{1\mathrm{SWIR}} f_1(\theta_{vi}, \theta_{si}, \phi_i) + a_{2\mathrm{SWIR}} f_2(\theta_{vi}, \theta_{si}, \phi_i)) \cdot \left(1 + c_{1\mathrm{SWIR}} \exp\left[\left(\frac{\xi_i}{\pi}\right) c_{2\mathrm{SWIR}}\right]\right)} \tag{12}$$

$$L = f_{\mathrm{L\_RSR}} \left(\mathrm{SR} \cdot f_{\mathrm{BRDF}}(\theta_v, \theta_s, \phi, a_1(L), a_2(L)) \cdot \left(1 - \frac{\rho_{\mathrm{SWIR}} \cdot f_{\mathrm{SWIR\_BRDF}}(\theta_v, \theta_s, \phi, a_1(L), a_2(L)) - \rho_{\mathrm{SWIR\,min}}}{\rho_{\mathrm{SWIR\,max}} - \rho_{\mathrm{SWIR\,min}}}\right)\right) \tag{14}$$

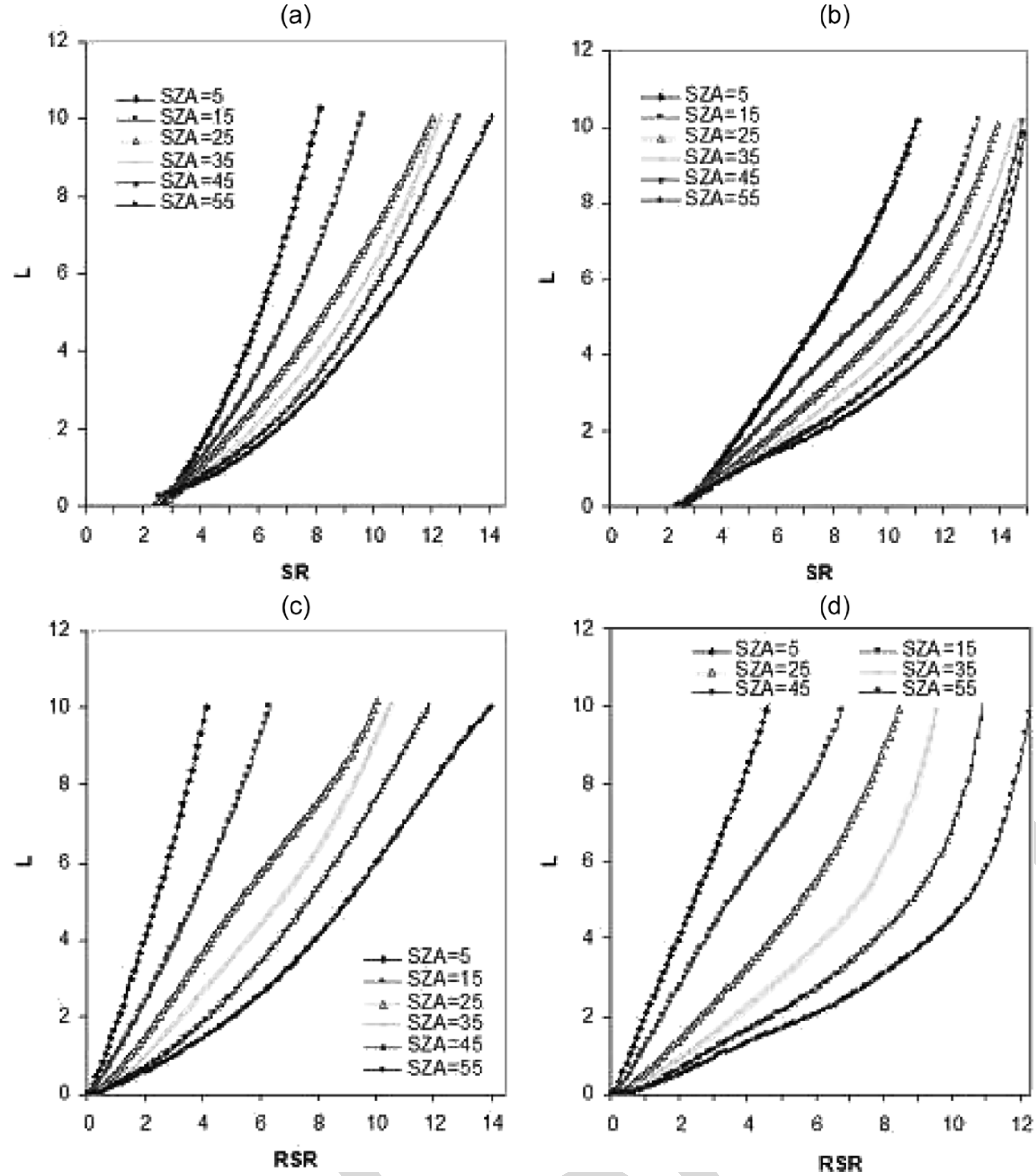

Fig. 1. L–SR and L–RSR relationships for the coniferous and deciduous types at a fixed view angle (nadir) but at different SZAs.

The modified Roujean's model is used as a base to fit the results of each of the calculated reflectances to determine c_1 and c_2 and, at the same time, to apply Chebyshev polynomials of the second kind to fit to the simulated coefficients a_1 and a_2 as functions of LAI. The relationship of LAI with SR or RSR is also fitted using the same polynomials. Relationships between L and SR $(f_{\mathrm{L\_SR}})$ and between L and RSR $(f_{\mathrm{L\_RSR}})$ at selected angle combinations for coniferous and deciduous forests are shown in Fig. 1 as examples. These four figures demonstrate the following points: 1) Changes in the SZA have large effects on the L–SR and L–RSR relationships for both coniferous and deciduous cover types, suggesting that considering SZA in LAI algorithms is very important; 2) the relationships for the coniferous forest type are more linear than those for deciduous forest types, in agreement with experimental findings of Chen *et al.* [9]; 3) L–RSR curves are further apart than L–SR curves at different SZAs, indicating that after considering SWIR in RSR, the influence of SZA is enhanced. This may be due to a large angle dependence of the reflectance in the SWIR band; and 4) at larger SZAs, the saturations of SR and RSR at LAI > 6 are more apparent for the deciduous forest type, also in agreement with empirical evidence of Chen *et al.* [9]. Relationships between L and SR $(f_{\mathrm{L\_SR}})$ and between L and RSR $(f_{\mathrm{L\_RSR}})$ for different cover types at specific angle combinations are shown in Fig. 2. From these figures, we see that although the LAI of the coniferous type increases quickly with increasing SR, it is relatively slow for crops and grass. The other cover types are the intermediate cases. These differences reflect the effects of the canopy structure (such as foliage clumping) and the optical characteristics of leaves in each cover type. Comparing Fig. 2(a) and (b), we can see that the differences in L–RSR relationships for the various cover types are much smaller than those in L–SR relationships, suggesting a smaller cover type dependence of the

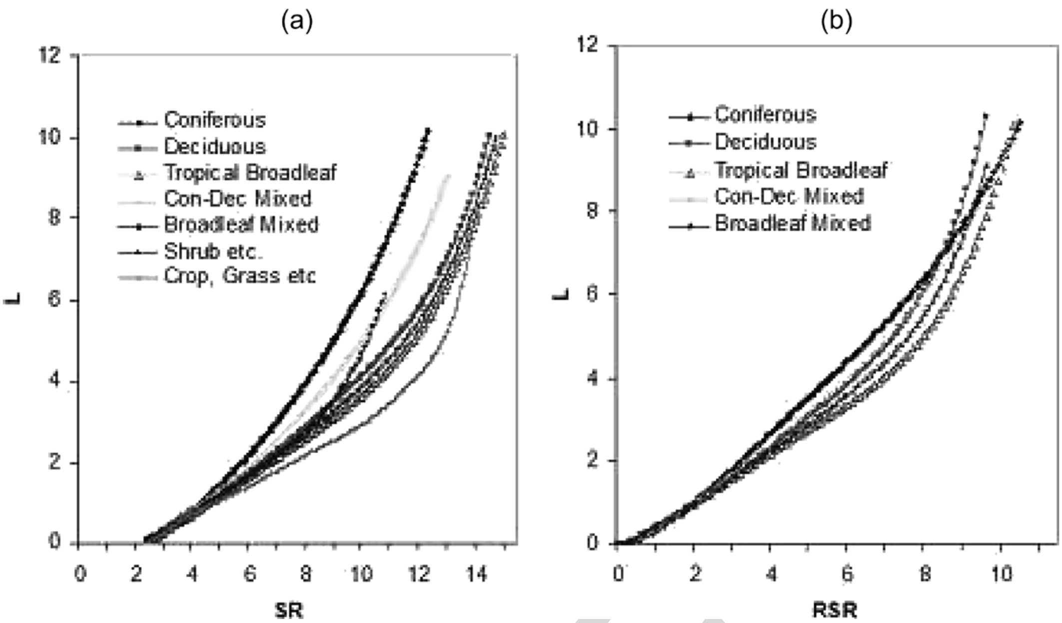

Fig. 2. L–SR and L–RSR relationships for different cover types at nadir and at SZA of 35°.

RSR [25]. However, the differences among various cover types in Fig. 2(b) are still significant, and therefore, a land cover-dependent algorithm is still a necessary even if RSR is used.

D. Implementation Procedure

In applying the LAI algorithm, the following steps are followed:

Step 1) The SZA is divided into six ranges, i.e., 1) [0, 10], 2) [10, 20], 3) [20, 30], 4) [30, 40], 5) [40, 50], 6) [50, 70], and for each SZA range, a set of relationships between L and SR ($f_{\mathrm{L\_SR}}$) are provided at different VZAs: 0°—representing a VZA range of [0, 10], 20°—representing a VZA range of [10, 20], 30°—representing a VZA range of [30, 45], and 50°—representing a VZA range of larger than 45°, at two azimuth angles between the sun and the viewer (ϕ): 0° and 180°. A linear interpolation is performed to obtain a final relationship at a given ϕ value for the first approximation of L.

Step 2) For each SZA range, predefined $a_1(L)$ and $a_2(L)$ functions in the form of Chebyshev polynomials of the second kind and parameters c_1 and c_2 are used to calculate the relevant f_{BRDF} and $f_{\mathrm{SWIR\_BRDF}}$, so we can estimate SR and RSR at any angle combinations.

Step 3) LAI is calculated using the relationships between L and SR ($f_{\mathrm{L\_SR}}$) and between L and RSR ($f_{\mathrm{L\_RSR}}$) at specific angles.

The general flowchart and a detail procedure for calculating the LAI are shown in Figs. 3 and 4, respectively.

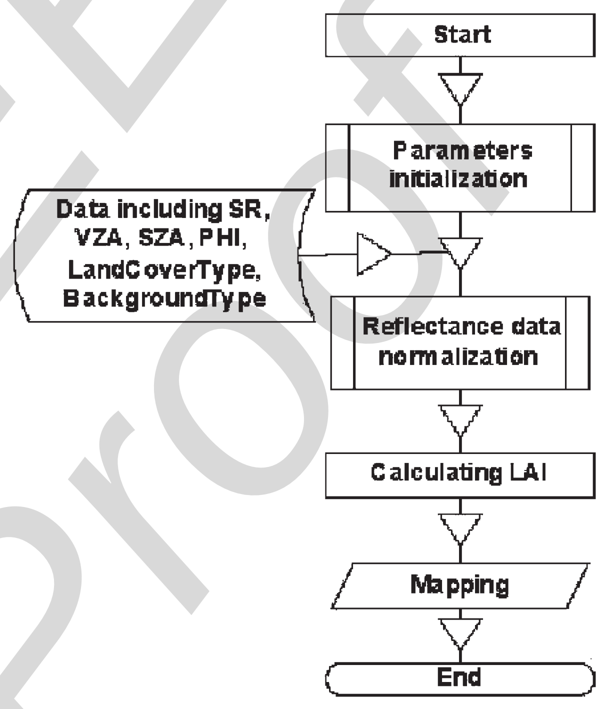

Fig. 3. General flowchart for the LAI algorithm.

E. SR- and RSR-Based Algorithms

As described in the last two sections, we have developed two separate algorithms, i.e., 1) SR based and 2) RSR based, to retrieve LAI. These algorithms can produce two separate maps of LAI for a given satellite image. As RSR was developed to minimize the variable background effect on LAI retrieval for forest stands and is sensitive to rainfall or irrigation in cropland and grassland [9], the RSR algorithm is used for all forest pixels and the SR algorithm for all other cover types to produce one LAI map for a given input image. These two separate algorithms also give a freedom for their applications to sensors with and without the SWIR band.

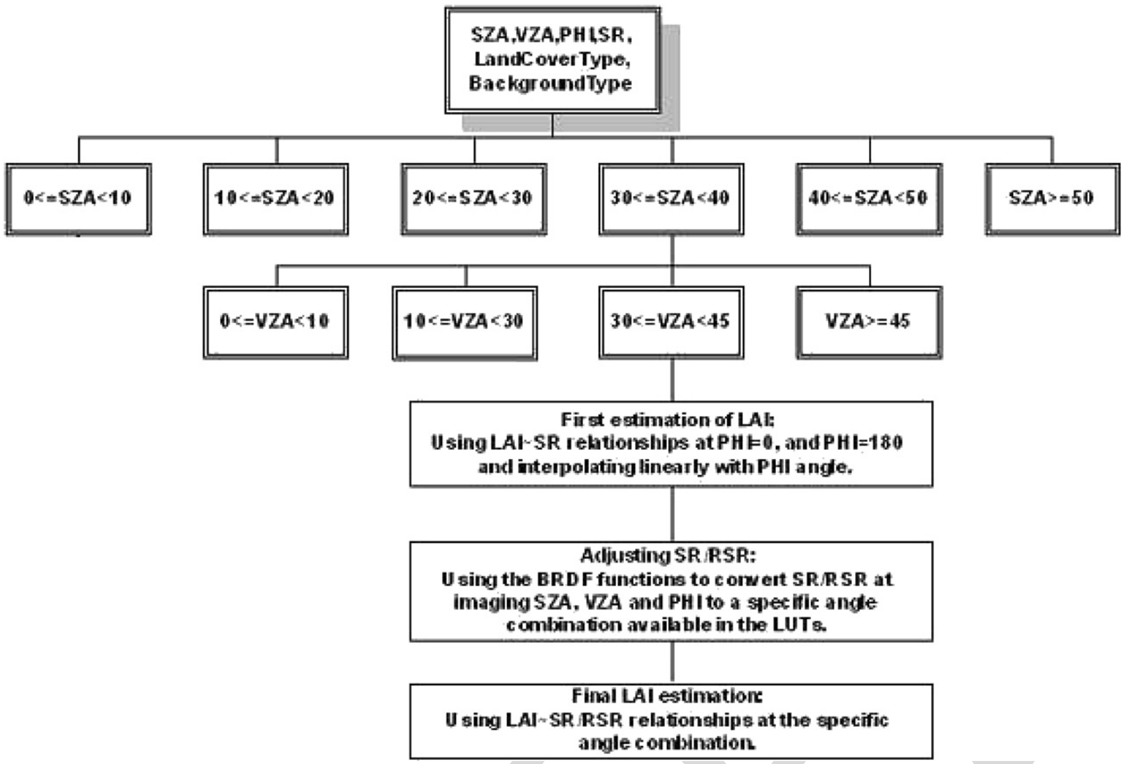

Fig. 4. Procedure to calculate LAI. For a given pixel in the image processing, only one SZA range and one VZA range are selected at a time to complete the procedure.

IV. Results—Global LAI Example Maps

Based on this new LAI algorithm, VEGETATION 10-day synthesis images have been used to produce global LAI maps. As examples, images dated January 21 and July 21, 2003 are used to produce the two LAI maps shown in Fig. 5. The spatial patterns and general LAI magnitudes are comparable to those produced by Myneni *et al.* [18]. These VEGETATION S10 images have been adjusted for the atmospheric effect using the Simplified Method for Atmospheric Correction (SMAC) [37], and clouds were screened using the standard VEGETATION formulas. However, despite these approaches and the use of maximum NDVI criterion for selecting the best date of measurements in each pixel to form the 10-day synthesis, it is still possible to find considerable residual cloud effects. The low LAI areas in part of the Amazon, for example, are caused by these effects. To minimize these effects, we have developed a procedure named locally adjusted cubic-spline capping (LACC) [20] to reconstruct the seasonal trajectory of LAI pixel by pixel. The LACC procedure is designed to produce a seasonal capping curve by progressively replacing abnormally low values with fitted values. As the application of this procedure requires a full seasonal series of images, it has not been applied to these two examples.

V. Accuracy Assessment

The accuracy assessment was conducted in three parts, namely: 1) the accuracy of the two-kernel Chebyshev approximation is examined to see how well the algorithm reflects the forward modeling; 2) the resulting LAI estimates are compared against an existing validated product for Canada; and 3) a comparison is made with ground measurements in 1998 in seven Landsat scenes in Canada.

A. Model Inversion Accuracy

In the complete inversion process, we used a simple two-kernel model to fit results simulated by the complex Four-Scale model, and some of the fitted coefficients are expressed in Chebyshev polynomials. Each step is a simplification of physical processes into mathematical descriptions and can induce errors. We therefore need to assess the size of these errors. Deciduous and coniferous cover types are selected to represent the whole inversion accuracy analysis because we treat every cover type with the same physical and mathematical methods. For deciduous and coniferous cover types, 12 486 and 17 128 groups of simulation results, including the angle combinations, background reflectances, and canopy-level reflectances for different LAI levels that are obtained from the input and output datasets of Four-Scale simulations, are used as inputs to the LAI algorithm to calculate LAI values, and these LAI values are statistically processed to compare with the input LAI values to the Four-Scale model. Fig. 6 presents the inverted LAI mean values and related standard deviation (SD) from the algorithm as compared with the corresponding LAI inputs to the forward Four-Scale model.

As demonstrated in Fig. 6, this new algorithm has extracted most of the information from the complex model. Statistically, this algorithm gives fairly acceptable LAI values compared with the input LAI of the complex model with a maximum

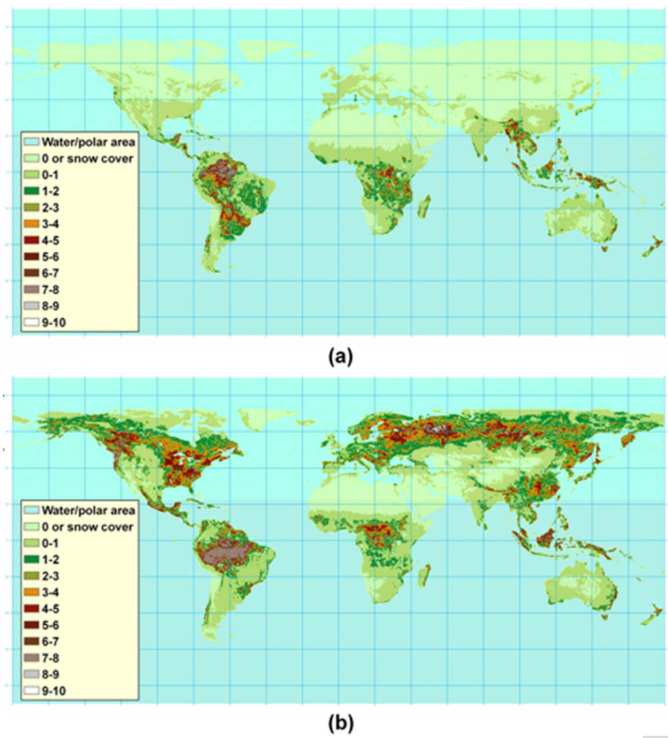

Fig. 5. Global LAI map produced from a cloud-free 10-day synthesis image of VEGETATION for the period of (a) January 21–31 and (b) July 21–31, 2003.

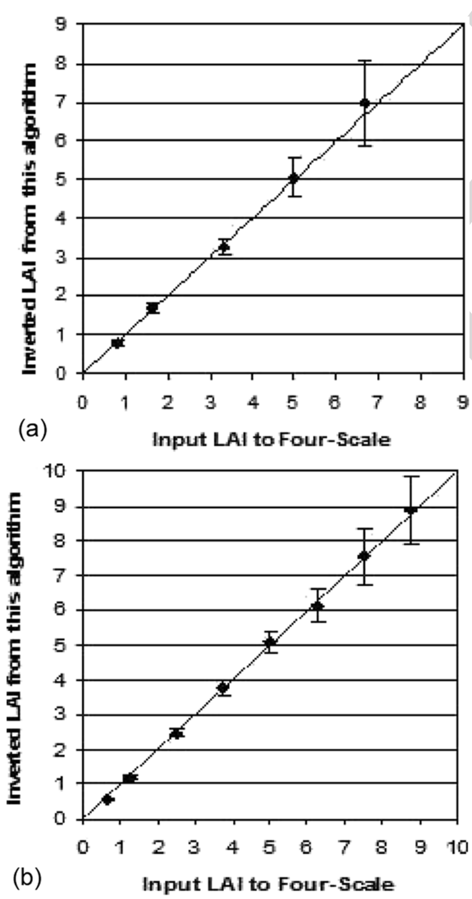

Fig. 6. Mean values of inverted LAI from the current algorithm versus the input LAI to the Four-Scale model for (a) deciduous and (b) coniferous cover types. The bar over each mean value represents the standard deviation of related LAI sample.

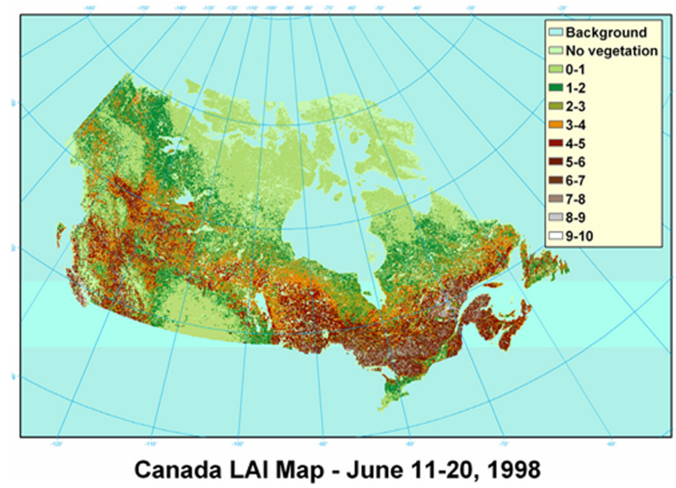

Fig. 7. Canada-wide LAI map produced from a cloud-free 10-day synthesis image of VEGETATION for the period of June 11–20, 1998.

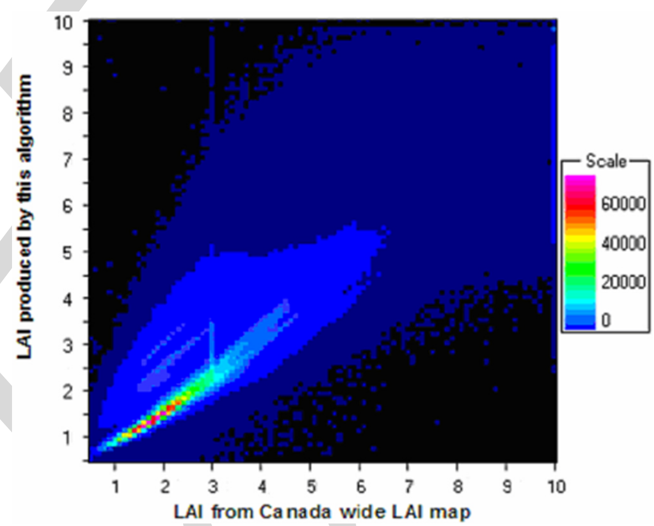

Fig. 8. Canada-wide LAI map [9] versus a new LAI map (Fig. 8) produced using the current algorithm. Both images were produced from the same cloud-free 10-day synthesis image of VEGETATION for the period of June 11–20, 1998.

SD of 15% and 11% for deciduous and coniferous cover types, respectively. Standard errors would be about 120 times smaller.

B. Canada-Wide LAI Map Comparison

To ensure that our new algorithm are practical and are able to produce LAI maps of desired accuracy, a VEGETATION 10-day synthesis image dated June 11, 1998 was used here to produce the Canada-wide LAI map shown in Fig. 7 using the new algorithm. The same image was previously used to produce a Canada-wide LAI map with a different algorithm requiring inputs of BRDF-normalized surface reflectance. This existing LAI map has undergone significant evaluation against ground measurements [9]. A 1:1 scatter plot between the existing and the current LAI maps of all cover types is shown in Fig. 8, indicating a satisfactory agreement between these two maps produced with different algorithms (the correlation coefficient is 0.86). The apparent vertical line at $\mathrm{LAI} = 3$ in Fig. 8 is caused by an artificial limit of $\mathrm{LAI} = 3$ for grassland imposed

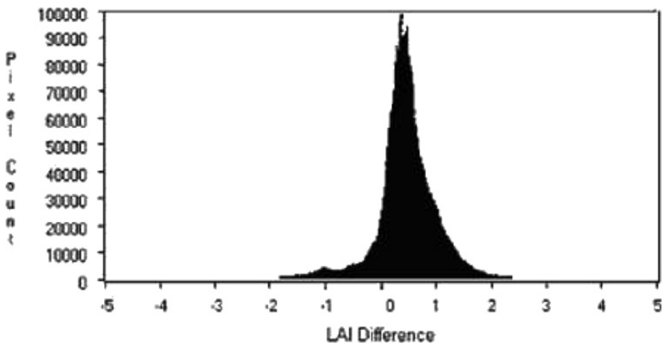

Fig. 9. Histogram of the difference in LAI between the new Canada-wide LAI map (Fig. 8) and the previous map [9].

in the previous algorithm of Chen *et al.* [9], but no such a limit is used in the current algorithm. In the mean time, a histogram of the difference between these two LAI maps is presented in Fig. 9, where a positive value on the horizontal axis indicates a larger value from the previous algorithm than from the current algorithm. The mean difference between these two maps is less than 0.5 with an SD of 0.4. At high LAI values (LAI > 7, Fig. 8), there is a tendency that the values in the new LAI map shown in Fig. 7 are smaller than the corresponding values in the map of Chen *et al.* [9]. This discrepancy in LAI is caused by a difference between the algorithms for the conifer type. In Chen *et al.* [9], an empirical linear relationship between RSR and LAI was used for conifer, whereas in the new algorithm, this relationship is slightly curvilinear (Fig. 2), making LAI increase slower at larger RSR values. Based on the physics of radiation interaction with the canopy, the curvilinear shape is expected at high LAI values.

C. Validation Against Ground LAI Measurements

The current LAI algorithm was validated indirectly against ground-based LAI data using seven fine-resolution (30 m) LAI images derived from Landsat TM scenes, covering different biomes in Canada. Using high-resolution images was a necessary step in validating coarse-resolution LAI images against the ground data because ground plots were generally smaller than 100 m in width or length. Ground measurements were made in 1998 in these scenes by a large group using common instruments and measurement protocols [9]. These LAI images at 30-m resolution were retrieved using empirical relationships established based on ground measurements and aggregated to 1-km resolution, as compared with the VEGETATION LAI image (Fig. 7) calculated based on GLC2000 land cover data. To minimize the effects of differences in land cover classification between GLC2000 at 1-km resolution and that of Landsat images at 30-m resolution, three VEGETATION LAI images were retrieved with three different methods in using land cover information, namely: 1) the original GLC2000 dataset was used without any modifications; 2) the dominant land cover type for each 1-km pixel was used based on Landsat land cover information [9]; and 3) the fractions of various land cover types in the Landsat images were used to weight the individual LAI values corresponding to the different cover types. These three LAI images were compared with Landsat LAI images,

TABLE II

AVERAGE (AVG.) AND SD OF LAI FOR EACH LANDSAT TM SCENE AND COEFFICIENTS OF DETERMINATION (r^2), ROOT-MEAN-SQUARE ERROR (RMSE), AND MEAN BIAS (MB) OF EACH OF THE THREE VEGETATION (VGT) LAI RESULTS AT 1-km RESOLUTION AGAINST THESE LANDSAT SCENES. THE THREE VGT RESULTS CORRESPOND TO THREE DIFFERENT TREATMENTS OF LAND COVER INFORMATION, NAMELY: 1) USING THE ORIGINAL GLCC LAND COVER INFORMATION ($\mathrm{LC_{GLCC}}$); 2) USING THE DOMINANT LAND COVER INFORMATION ($\mathrm{LC_{dominant}}$) BASED ON LANDSAT IMAGES; AND 3) WEIGHTED LAI ($\mathrm{LC_{weighted}}$) FOR LAND COVER FRACTIONS IN THE LANDSAT IMAGES

		Victoria	Acadia	Ottawa	Ontario	Radisson	Kanaskasis	Whitecourt
TM	Avg.	3.97	3.94	3.22	3.55	1.31	3.21	3.2
	SD	3.17	1.46	0.95	1.16	0.50	1.31	1.03
VGT ($\mathrm{LC_{GLCC}}$)	r^2	0.75	0.54	0.44	0.13	0.17	0.55	0.23
	RMSE	1.72	1.09	0.88	1.59	0.68	0.89	1.27
	MB	0.28	0.41	0.17	2.79	0.34	-0.91	-0.98
VGT ($\mathrm{LC_{dominant}}$)	r^2	0.82	0.65	0.52	0.26	0.45	0.67	0.43
	RMSE	1.47	0.87	0.96	1.25	0.45	0.75	0.89
	MB	0.02	0.01	0.2	2.05	0.06	-0.85	-0.84
VGT ($\mathrm{LC_{weighted}}$)	r^2	0.85	0.76	0.55	0.50	0.60	0.70	0.50
	RMSE	1.30	0.72	0.83	1.10	0.34	0.71	0.79
	MB	-0.19	-0.13	0.36	1.53	-0.03	-0.82	-0.92

and statistics of these comparisons are summarized in Table II. The coefficients of determination for the VEGETATION LAI image derived using the first method were quite variable among the scenes ($r^2 = 0.13-0.75$). Significant improvements were achieved ($r^2 = 0.26-0.82$) when the second method was used. The best results were found using the third method ($r^2 = 0.50-0.85$). These results suggest that the correct use of land cover information played a vital role in LAI mapping, and when accurate land cover information in the detailed Landsat scenes were used, the algorithm applied to the VEGETATION image produced LAI values in good agreement with Landsat scenes. This reaffirms the finding of Chen [38] that downscaling using subpixel land cover information can considerably increase the LAI mapping accuracy. This is especially true for Ontario and Radisson scenes, where the land covers were more mixed than the other scenes. A significant portion of the remaining errors can be further explained by errors due to other factors (e.g., nonlinearity in the LAI algorithm) and differences in input VIs between these high- and low-resolution images. These validation results suggest that the current LAI algorithm produced reliable results for various cover types including deciduous and conifer forests, crops, and grassland.

VI. CONCLUSION

The new LAI algorithm presented here features several desirable characteristics for global application.

1) The two models (Four-Scale and two kernel) used in our algorithm development are based on radiative transfer physics rather than on empirical curve or surface fitting techniques, so that the algorithm provides the fundamental trends of LAI variations with remote sensing signals for various land cover types.
2) The procedure of angular normalization to the input reflectance images is no longer needed as the new algorithm makes direct use of the measurements at all angles. The angular variations of remote sensing signals are no longer treated as sources of noise but rather sources of

information, provided the angular patterns for various cover types are modeled accurately. In addition, without the need for the angular normalization, which is difficult for applications to the globe where the SZA varies greatly within a given date, this new algorithm is suitable for both regional and global applications.

3) With the emphasis on large-area applications, small LUTs requiring only two iterations are used instead of a time-consuming exact numerical method, so that this algorithm is computationally highly efficient without sacrificing the accuracy of LAI retrieval. It is now feasible to produce global LAI images at 1-km resolution on a personal computer (for a whole globe image at one date, it requires 12 h with a Pentium 4 PC at 3.0 GHz).

The simplified inversion algorithm is shown to be able to reproduce the LAI values used as input to the forward model. The resulting spatial estimate for Canada compares favorably with a previously validated Canada-wide LAI map and ground measurements in seven Landsat scenes in Canada. Further work is needed to validate the algorithm for other regions of the globe.

Acknowledgment

The authors thank Dr. O. Arino of the European Space Agency (ESA) for providing valuable suggestions at the early phase of the algorithm development. This LAI algorithm is developed as part of the GLOBCARBON project of ESA.

References

[1] G. B. Bonan, F. S. Chapin, and S. L. Thompson, "Boreal forest and tundra ecosystems as components of the climate system," *Clim. Change*, vol. 29, no. 2, pp. 145–167, Feb. 1995.

[2] J. W. Rouse, R. H. Haas, J. A. Schell, and D. W. Deering, "Monitoring vegetation systems in the great plains with ERTS," in *Proc. 3rd Earth Resources Technol. Satellite-1 Symp.*, Greenbelt, MD, 1974, pp. 309–317.

[3] C. F. Jordan, "Derivation of leaf-area index from quality of light on the forest floor," *Ecology*, vol. 50, no. 4, pp. 663–666, 1969.

[4] J.-L. Roujean and F. M. Breon, "Estimating PAR absorbed by vegetation from bidirectional reflectance measurements," *Remote Sens. Environ.*, vol. 51, no. 3, pp. 375–384, Mar. 1995.

[5] J. M. Chen, "Evaluation of vegetation indices and a modified simple ratio for boreal application," *Can. J. Remote Sens.*, vol. 22, no. 3, pp. 229–242, 1996.

[6] A. R. Huete, "A soil-adjusted vegetation index (SAVI)," *Remote Sens. Environ.*, vol. 25, no. 3, pp. 295–309, Aug. 1988.

[7] P. J. Sellers, S. O. Los, C. J. Tucker, C. O. Justice, D. A. Dazlich, G. J. Collatz, and D. A. Randall, "A revised land surface parameterized (SiB2) for atmospheric GCMs: II. The generation of global fields of terrestrial biophysical parameters from satellite data," *J. Climate*, vol. 9, no. 4, pp. 706–737, 1996.

[8] R. B. Myneni, R. R. Nemani, and S. W. Running, "Estimation of global leaf area index and absorbed PAR using radiative transfer models," *IEEE Trans. Geosci. Remote Sens*, vol. 35, no. 6, pp. 1380–1393, Nov. 1997.

[9] J. M. Chen, G. Pavlic, L. Brown, J. Cihlar, S. G. Leblanc, H. P. White, R. J. Hall, D. R. Peddle, D. J. King, J. A. Trofymow, E. Swift, J. Van der Sanden, and P. K. E. Pellikka, "Derivation and validation of Canada-wide coarse-resolution leaf area index maps using high-resolution satellite imagery and ground measurements," *Remote Sens. Environ.*, vol. 80, no. 1, pp. 165–184, Apr. 2002.

[10] J. Cihlar, J. M. Chen, and Z. Li, "Seasonal AVHRR multichannel data sets and products for studies of surface—Atmosphere interactions," *J. Geophys. Res.*, vol. 102, no. D24, pp. 29625–29640, 1997.

[11] J. Liu, J. M. Chen, J. Cihlar, and W. Chen, "Net primary productivity distribution in the BOREAS study region from a process model driven by satellite and surface data," *J. Geophys. Res.*, vol. 104, no. D22, pp. 27735–27754, 1999.

[12] J. Liu, J. M. Chen, J. Cihlar, and W. Park, "A process-based boreal ecosystems productivity simulator using remote sensing inputs," *Remote Sens. Environ.*, vol. 62, no. 2, pp. 158–175, Nov. 1997.

[13] N. Goel, "Inversion of canopy reflectance models for estimation of biophysical parameters from reflectance data," in *Theory and Applications of Optical Remote Sensing*, G. Asrar, Ed. New York: Wiley, 1989, pp. 205–250.

[14] P. Bicheron and M. Leroy, "A method of biophysical parameter retrieval at global scale by inversion of a vegetation reflectance model," *Remote Sens. Environ.*, vol. 67, no. 3, pp. 251–266, Mar. 1999.

[15] C. Bacour, S. Jacquemoud, M. Leroy, O. Hautecoeur, M. Weiss, L. Prévot, L. Bruguier, and H. Chauki, "Reliability of the estimation of vegetation characteristics by inversion of three canopy reflectance models on airborne POLDER data," *Agronomie: Agric. Environ.*, vol. 22, no. 6, pp. 555–565, 2002.

[16] N. Gobron, B. Pinty, M. M. Verstraete, J. V. Martonchik, Y. Knyazikhin, and D. J. Diner, "Potential of multiangular spectral measurements to characterize land surfaces: Conceptual approach and exploratory application," *J. Geophys. Res.—Atmos.*, vol. 105, no. D13, pp. 17539–17549, 2000.

[17] M. Weiss, F. Baret, R. B. Myneni, A. Pragnère, and Y. Knyazikhin, "Investigation of a model inversion technique to estimate canopy biophysical variables from spectral and directional reflectance data," *Agronomie*, vol. 20, no. 1, pp. 3–22, 2000.

[18] R. B. Myneni, S. Hoffman, Y. Knyazikhin, J. L. Privette, J. Glassyc, Y. Tian, Y. Wang, X. Song, Y. Zhang, G. R. Smith, A. Lotsch, M. Friedl, J. T. Morisette, P. Votava, R. R. Nemani, and S. W. Running, "Global products of vegetation leaf area and fraction absorbed PAR from year one of MODIS data," *Remote Sens. Environ.*, vol. 83, no. 1/2, pp. 214–231, Nov. 2002.

[19] A. Lotsch, Y. Tian, M. A. Friedl, and R. B. Myneni, "Land cover mapping in support of LAI/FPAR retrievals from EOS-MODIS and MISR: Classification methods and sensitivities to errors," *Int. J. Remote Sens.*, vol. 24, no. 10, pp. 1997–2016, May 2003.

[20] J. M. Chen, F. Deng, and M. Chen, "Locally adjusted cubic-spline capping for reconstructing seasonal trajectories of a satellite-derived surface parameter," *IEEE Trans. Geosci. Remote Sens.*, 2006. In press.

[21] J. Cihlar, H. Ly, Z. Li, J. Chen, H. Pokrant, and F. Huang, "Multitemporal, multichannel AVHRR data sets for land biosphere studies: Artifacts and corrections," *Remote Sens. Environ.*, vol. 60, no. 1, pp. 35–57, Apr. 1997.

[22] J. M. Chen and S. Leblanc, "A 4-scale bidirectional reflection model based on canopy architecture," *IEEE Trans. Geosci. Remote Sens.*, vol. 35, no. 5, pp. 1316–1337, Sep. 1997.

[23] J. M. Chen and T. A. Black, "Defining leaf area index for non-flat leaves," *Plant Cell Environ.*, vol. 15, no. 4, pp. 421–429, 1992.

[24] J. Ross, *The Radiation Regime and Architecture of Plan Stands*. Hague, The Netherlands: Dr. W. Junk Publishers, 1981.

[25] L. J. Brown, J. M. Chen, S. G. Leblanc, and J. Cihlar, "Short wave infrared correction to the simple ratio: An image and model analysis," *Remote Sens. Environ.*, vol. 71, no. 1, pp. 16–25, Jan. 2000.

[26] W. Qin and S. Liang, "Plane-parallel canopy radiation transfer modeling: Recent advances and future directions," *Remote Sens. Rev.*, vol. 18, no. 2–4, pp. 281–306, Dec. 2000.

[27] J. M. Chen, X. Li, T. Nilson, and A. Strahler, "Recent advances in geometrical optical modelling and its applications," *Remote Sens. Rev.*, vol. 18, no. 2–4, pp. 227–262, Dec. 2000.

[28] J. M. Chen and S. G. Leblanc, "Multiple-scattering scheme useful for hyperspectral geometrical optical modelling," *IEEE Trans. Geosci. Remote Sens.*, vol. 39, no. 5, pp. 1061–1071, May 2001.

[29] P. H. White, J. R. Miller, and J. M. Chen, "Four-scale linear model for anisotropic reflectance (FLAIR) for plant canopies. I: Model description and partial validation," *IEEE Trans. Geosci. Remote Sens.*, vol. 39, no. 5, pp. 1073–1083, May 2001.

[30] ——, "Four-scale linear model for anisotropic reflectance (FLAIR) for plant canopies—Part II: Validation and inversion with CASI, POLDER and PARABOLA data at BOREAS," *IEEE Trans. Geosci. Remote Sens.*, vol. 40, no. 5, pp. 1038–1046, May 2002.

[31] J. M. Chen and J. Cihlar, "A hotspot function in a simple bidirectional reflectance model for satellite applications," *J. Geophys. Res.*, vol. 102, no. D22, pp. 25907–25913, 1997.

[32] J.-L. Roujean, M. Leroy, and P.-Y. Deschamps, "A bidirectional reflectance model of the earth's surface for the correction of remote sensing data," *J. Geophys. Res.*, vol. 97, no. D8, pp. 20455–20468, 1992.

[33] M. T. Heath, *Scientific Computing, An Introductory Survey*, 2nd ed. New York: McGraw-Hill, 2002, p. 232.

[34] "Orthogonal polynomials," in *Handbook of Mathematical Functions With Formulas, Graphs, and Mathematical Tables*, M. Abramowitz and I. A. Stegun, Eds. New York: Dover, 1972, ch. 22, pp. 771–802.

[35] USGS Land Processes Distributed Active Archive Center, *Global Land Cover Characteristics Data Base*. [Online]. Available: http://edcdaac.usgs.gov/glcc/glcc.asp

[36] European Commission, Joint Research Centre, *Global Land Cover 2000 Database,* 2003. [Online] Available: http://www.gvm.jrc.it/glc2000

[37] H. Rahman and G. Dedieu, "SMAC: A simplified method for the atmospheric correction of satellite measurements in the solar spectrum," *Int. J. Remote Sens.*, vol. 15, no. 1, pp. 123–143, 1994.

[38] J. M. Chen, "Spatial scaling of a remote sensed surface parameter by contexture," *Remote Sens. Environ.*, vol. 69, no. 1, pp. 30–42, Jul. 1999.

Feng Deng received the B.S. and M.S. degrees in geography and climatology from the East China Normal University, Shanghai, China.

He was a Researcher at the Institute of Environmental Studies of Ningbo, China. He is currently with the Department of Geography and Planning Program, University of Toronto, Toronto, ON, Canada. His research interests are the application of remote sensing and geographic information system in the field of global changes.

Jing M. Chen received the B.Sc. degree from the Nanjing Institute of Meteorology, Nanjing, China, in 1982 and the Ph.D. degree in meteorology from Reading University, Reading, U.K., in 1986.

From 1989 to 1993, he was a Postdoctoral Fellow and Research Associate at the University of British Columbia, Vancouver, BC, Canada. From 1993 to 2000, he was a Research Scientist at the Canada Centre for Remote Sensing, Ottawa, ON. He is currently a Professor and a Canada Research Chair at the Department of Geography, University of Toronto, Toronto, ON, Canada, and an Adjunct Professor at York University, Toronto, ON, Canada. His recent research interests are in the remote sensing of biophysical parameters, plant canopy radiation modeling, terrestrial water and carbon cycle modeling, and atmospheric inverse modeling for global and regional carbon budget estimation. He has published over 120 papers in refereed journals.

Dr. Chen served as the Associate Editor of the IEEE TRANSACTIONS ON GEOSCIENCE AND REMOTE SENSING from 1996 to 2002.

Stephen Plummer. Please provide biographical information.

Mingzhen Chen received the Ph.D. degree in remote sensing of soils from Zhejiang University, Zhejiang, China.

From 1996 to 1998, he was an Associate Professor at Zhejiang University. From 1999 to 2001, he was a Visiting Research Scientist at the University of Maryland at College Park. He was a Research Associate previously at University of Toronto and currently at the Auburn University, Auburn, AL. His research interests include remote sensing and geographic information system (GIS) applications, such as retrieving land surface parameters from remotely sensed data, land cover and land use, digital image processing, natural resources inventory and management, biomass and environmental monitoring, and GIS system design and implementation.

Jan Pisek received the M.S. degree in geoinformatics and cartography from Masaryk University, Brno, the Czech Republic, in 2004, the M.Sc. degree in physical geography from the University of Toronto, Toronto, ON, Canada, in 2005, and is currently working toward the Ph.D. degree in physical geography at the University of Toronto, working on the retrieval of global fields of clumping index values and background understory reflectance and their incorporation with hyperspectral remote sensing information in the global coverage leaf area index algorithms.

His research interests cover remote sensing of the atmosphere and biosphere, especially information extraction from multiangular remote-sensed images and object-oriented image classification.

AUTHOR QUERIES

AUTHOR PLEASE ANSWER ALL QUERIES

AQ1 = Please provide the expanded form of the acronym "ENVISAT."
AQ2 = "NASA SP-351, 3010-317" in Ref. [2] was deleted. Please check.
AQ3 = "9th printing" in Ref. [34] was deleted. Please check.
AQ4 = Please provide additional information, if possible, in Ref. [35].
AQ5 = Please indicate the years the B.S. and M.S. degrees were earned.
AQ6 = Please specify major field of study (B.Sc. degree).
AQ7 = Please indicate the year the Ph.D. degree was earned.

END OF ALL QUERIES